Journal of
Composites Science

MDPI

Article

Synthesis of MRGO Nanocomposites as a Potential Photocatalytic Demulsifier for Crude Oil-in-Water Emulsion

Zhen Yin Lau [1], Ko Shyn Tan [1], Cheng Seong Khe [1,*], Chin Wei Lai [2], Kok Yeow You [3] and Wai Kian Tan [4]

[1] Department of Fundamental and Applied Sciences, Universiti Teknologi PETRONAS, Seri Iskandar 32610, Malaysia; lauzhenyin@gmail.com (Z.Y.L.); ko_20000993@utp.edu.my (K.S.T.)
[2] Nanotechnology & Catalysis Research Centre (NANOCAT), Institute for Advanced Studies (IAS), University of Malaya, Kuala Lumpur 50603, Malaysia; cwlai@um.edu.my
[3] Department of Communication Engineering, Faculty of Electrical Engineering, Universiti Teknologi Malaysia, Johor Bahru 81310, Malaysia; ykyeow@utm.my
[4] Institute of Liberal Arts and Sciences, Toyohashi University of Technology, Toyohashi, Aichi 441-8580, Japan; tan@las.tut.ac.jp
* Correspondence: chengseong.khe@utp.edu.my; Tel.: +60-5368-7650

Abstract: Oil-in-water (O/W) emulsion has been a major concern for the petroleum industry. A cost-effective magnetite-reduced graphene oxide (MRGO) nanocomposite was synthesized to study the demulsification process of emulsion using said nanocomposite under solar illumination. Characterization data show that the magnetite was successfully deposited on reduced graphene oxide through redox reaction at varying loading amounts of magnetite. Demulsification of the O/W emulsion using MRGO nanocomposite shows that in general the demulsification efficiency was dependent on the loading amount of Fe_3O_4 on the RGO sheet. It was proposed that the surfactant hydroxyl groups have an affinity towards Fe_3O_4, which the loading amount was directly proportionate to available active site in Fe_3O_4. As the loading amount increases, charge recombination centers on the RGO sheet would increase, effectively affecting the charge distribution within MRGO structure.

Keywords: magnetite-reduced graphene oxide; photocatalytic demulsification; crude oil-in-water emulsion

Citation: Lau, Z.Y.; Tan, K.S.; Khe, C.S.; Lai, C.W.; You, K.Y.; Tan, W.K. Synthesis of MRGO Nanocomposites as a Potential Photocatalytic Demulsifier for Crude Oil-in-Water Emulsion. *J. Compos. Sci.* **2021**, *5*, 174. https://doi.org/10.3390/jcs5070174

Academic Editor: Jian-Zhang Chen

Received: 2 June 2021
Accepted: 30 June 2021
Published: 4 July 2021

1. Introduction

The oil and gas industry is one of the sectors with the heaviest industrialized resources in the world and the petroleum industry has long been faced with multitude of problems to improve the profitability and production. One of the issues is that the oily wastewater in the industries contains emulsion of water and oil liquids which was formed during the crude oil extraction process. Emulsions are classified into two classes, and the one focused in this work is oil-in-water (O/W) emulsion. O/W emulsion contains oil droplets encapsulated by the water matrix or dispersed water or surfactant forming an interfacial film at the oil and water interface which emulsifies the two immiscible liquids [1]. Emulsions have been a major concern in the petroleum industry as it affects the production and the pipeline system in the production [2]. Hence, in this work, a magnetite–carbon-based nanocomposite is studied for its efficiency and efficacy in demulsifying O/W emulsion.

Graphene, a revered material for its adsorption properties and in-plane conductivity, has shown excellent results in photocatalytic effect when composited with other materials [3]. Graphene oxide (GO) sheets has a π-π stacking within its sp^2 hybridized network and due to their large surface area and broad sp^2 network, they are promising material for organic compounds photodegradation [4] and demulsification [5]. However, separation of the material and recyclability has been an issue for graphene-based nanocomposites. To solve the separation issue, magnetite was suggested as Fe_3O_4 has shown excellent photocatalytic properties in organic compounds degradation [6] and the recyclability of the material has been promising [7]. Some previous studies [8–10] have shown that magnetite

(Fe_3O_4) materials have favorable properties due to their low degree of cytotoxicity and good biocompatibility, especially during synthesis with surface coatings. In addition, magnetite has shown excellent adsorptive properties on organic compounds [11]. However, Fe_3O_4 has a strong tendency to agglomerate [12] and that is a major concern as it would inhibit the photocatalytic and adsorptive properties.

By combining both GO and Fe_3O_4 through deposition of magnetite on GO sheets through redox reaction, the magnetite-reduced graphene oxide (MRGO) nanocomposite shows improved stability and higher adsorption rate than pristine GO sheets and Fe_3O_4 nanoparticles [13]. The MRGO nanocomposite prevents both problems with the agglomeration of Fe_3O_4 nanoparticles and the restacking of graphene sheets [14], and by reducing GO to reduced graphene oxide (RGO), it enhances the charge separation properties of the material, suppressing charge recombination at Fe_3O_4 active sites [15]. Through the synergy of both materials, MRGO nanocomposites show improved organic compounds degradation under sunlight irradiation [16].

Furthermore, MRGOs promised easy separation of nanocomposites from the emulsion through magnetic means, and the reusability and recyclability of the MRGOs have shown promising results as well, indicating that the MRGOs can be a cost-effective material for demulsification usage [17,18]. A high demulsification factor was observed when the interfacial film of the oil–water emulsion was significantly disrupted [19]. Hence, in this work, the demulsification process of O/W emulsion using MRGO nanocomposite under solar irradiation is studied. To our knowledge, the use of MRGO as a photocatalytic demulsifier for crude oil-in-water emulsion has not been reported yet.

2. Materials and Methods

2.1. Material

Graphite powder (99.99%) was purchased from Sigma Aldrich, USA. Sulfuric acid (H_2SO_4, 98%), phosphoric acid (H_3PO_4, 85%), potassium permanganate ($KMnO_4$, 99.9%), hydrogen peroxide (H_2O_2, 30%), hydrochloric acid (HCl, 37%), ammonia solution (NH_4OH, 25%), Iron (II) chloride ($FeCl_2 \cdot 6H_2O$), and surfactant Tween 60 were supplied by Merck, Germany. Tapis crude oil was obtained from Petronas Refinery at Melaka. Deionized water was used a Millipore Milli-Q water purification system with a resistivity of 18.2 MΩ cm^{-1}.

2.2. Synthesis of GO

GO was prepared and the magnetite-reduced graphene oxide was synthesized using an in situ chemical synthesis method [20]. An amount of 3 g of graphite flakes was oxidated with 400 mL of H_2SO_4, 40 mL of H_3PO_4 and 18 g of KMnO4 by using simplified Hummers' method [21]. The chemicals were mixed by using a magnetic stirrer and stirred for 5 min. However, the mixture was stirred for 3 days to ensure complete oxidation of graphite. During the oxidation, the color of mixture changed from dark purplish green to dark brown. H_2O_2 solution was added into the mixture to stop the oxidation process and the color of mixture changed to bright yellow, indicating a high degree of oxidation of graphite. The mixture solution was washed with 1 M of HCl aqueous solution and deionized water alternatively by using centrifugation techniques. The graphite oxide solids were obtained and dried.

2.3. Synthesis of MRGO Nanocomposites

MRGO nanocomposites were synthesized using different mass ratio of graphene oxides to irons salts, with the ratio of 1:5, 1:10 and 1:20, and differentiating the MRGOs as MRGO-5, MRGO-10 and MRGO-20, respectively.

The synthesis route for all MRGO nanocomposites was strictly maintained to be the same and only deionized water was used during the whole synthesis and experimental procedure.

Firstly, 0.5 g of graphene oxide was added into 200 mL of deionized water, and the GO aqueous suspension was ultrasonicated for 10 minutes or until all GO was finely

dispersed in the aqueous suspension. Once done, the GO suspension was placed onto a magnetic stirrer and the pH of the GO suspension was adjusted to about 11–12 using 25% ammonia solution added dropwise. Secondly, for MRGO-5, 2.5 g of $FeCl_2$ was dissolved in 100 mL of deionized water and added dropwise into the GO suspension. For MRGO-10 and MRGO-20, 5.0 g and 10.0 g of $FeCl_2$ were used, respectively.

The mixture solutions were then left for 12 h of stirring to ensure proper deposition of magnetite on GO to form MRGO nanocomposites. After 12 h, the black precipitation of the mixture solutions was extracted and washed with deionized water using a centrifuge. The centrifuge setting was 7000 rotations per minute with the rotation period of 10 minutes. The washing procedure was repeated for 3 times to wash out the extra ammonia present in the solution. The slurry was dried at 40 °C for 12 h, and the dried precipitation was grinded to obtain the powdered form of MRGO nanocomposites.

The entire process is repeated without GO to synthesize magnetite only through redox reaction in alkaline solution.

2.4. Preparation O/W Emulsion

The O/W emulsion is prepared by mixing 10 wt% of surfactant Tween 60, 10 wt% of Tapis crude oil and 80 wt% of deionized water. The physical and chemical properties of Tapis crude oil are tabulated in Tables 1 and 2, whereas Figure 1 shows the chemical formula of surfactant Tween 60. The mixed solution is then placed in a high-speed mixer for 10 utes to form the O/W emulsion.

Table 1. Physical properties of Tapis crude oil.

Parameter	Value
Density	0.827 g cm^{-3}
Viscosity	0.028 Pa s
API gravity	43.0
Surface Tension (at 30 °C)	30.30 mN m^{-1}
Interfacial Tension (at 30 °C)	28.80 mN m^{-1}

Table 2. Chemical properties of Tapis crude oil.

Parameter	Value (wt%)
Saturates	60.00
Aromatics	25.00
Resins	13.50
Asphaltenes	1.50

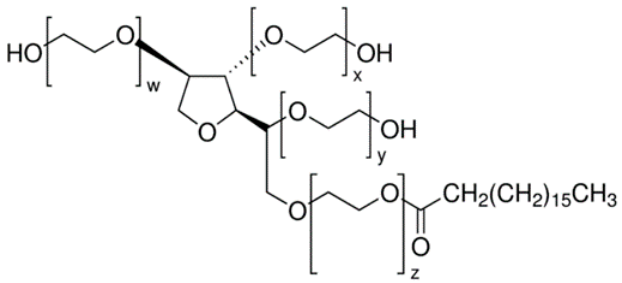

Figure 1. Chemical formula for Tween 60.

2.5. Characterization of MRGOs

An X-ray diffractometer (XRD Brucker D8 advance diffractometer) was used to verify the complete synthesis of GO and MRGOs with Cu Kα radiation (λ = 1.5406 A) in the

range of 2θ = 5°–80° with a step size 0.01°/step and exposure time 200 s/step. Then, Field-emission Scanning Electron Microscope (ZEISS Leo Supra 55, FESEM) was used to study the surface morphology of MRGO and verified the attachment of magnetite on the RGO sheets with an accelerating voltage of 5 kV. X-ray Photoelectron Spectroscopy (Thermo Scientific K-Alpha instrument, XPS) was used to study the composition information of GO and MRGOs. Measurements were used *Al* K_α ($h\nu$ = 1468.6 eV) as the radiation source. Further on, Fourier-transform Infra-red Spectrometer (Perkin Elmer Spectrum BX, FTIR) was used to determine the surface bonding of the synthesized GO and MRGOs with the wavelength range of 400–4000 cm^{-1}. Raman spectroscopy (Horiba Jabin Yvon HR800, RAMAN) was used to characterize the structural properties of synthesized MRGOs with 514.5 nm laser. Lastly, a vibrating sample magnetometer (DMS Model 10, VSM) was used to evaluate the magnetic properties of the synthesized MRGOs.

2.6. Demulsification Test

The test samples were prepared by mixing 1 mL of prepared O/W emulsion and 0.05 g of MRGOs into 19.4 mL of deionized water filled in a capped bottle. A standard solution without MRGO was prepared as well. The prepared test bottle samples were sonicated at a high intensity for 10 mins; where the MRGOs settled down at bottom of the bottle, the bottle should be swirled by hand to ensure proper distribution and mixing of the materials. After sonication, the bottles were mounted onto a vertical bottle shaker with 500 oscillation/min, under solar lamp illumination with varying intensities (0, 200, 400, 600, 800 and 1000 W/m^2) for 30 mins. The setup was as shown in Figure 2. Then, the bottles were removed from the shaker and placed on magnets for rapid settling of the MRGOs. The test samples were then left overnight on magnets for the mixture to stabilize at ambient conditions.

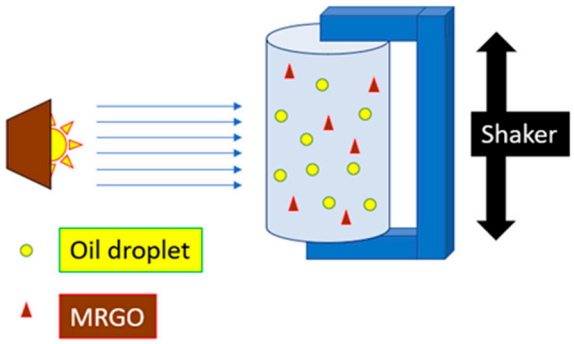

Figure 2. Schematic diagram of photocatalytic demulsification process.

The demulsification capability of MRGOs was determined by the residual oil content in the extracted water above the settled MRGO in the test samples. The oil concentration in standard and demulsified samples were obtained and compared from the standard curve of UV–visible absorption spectra by measuring the absorbance intensity at 228 nm. The demulsification efficiency under varying solar intensities was calculated by the following equation:

$$\text{Demulsification efficiency} = (1 - C_i/C_o) \times 100\%$$

where C_o is the initial concentration of oil content in the test sample and C_i represents the final concentration of oil content in the test sample.

3. Results and Discussion

3.1. XRD Analysis

Figure 3 displays the XRD patterns of GO, MRGO-5, MRGO-10 and MRGO-20; it shows the diffraction peak profiles of GO and MrGO from 5° to 75°. The characteristic peak of GO was observed at 10.3° corresponding to (001). However, for the MRGO

nanocomposites, there are six main characteristic peaks were observed at 20°, 30.2°, 43.4°, 53.7° and 62.8°, which are corresponding to diffraction indices of (220), (311), (400), (422), (511) and (440) crystal planes of Fe_3O_4 [22]. Additionally, peak intensities of Fe_3O_4 were observed to strengthen with the increase in the loading ratio of Fe_3O_4 on GO sheets, suggesting the successful deposition of Fe_3O_4 on RGO sheet through redox reaction at varying ratios. At high GO loading ratio, GO may hinder the crystallization of Fe_3O_4, while at a high Fe_3O_4 loading ratio, the XRD patterns are similar to only nanoparticles, as seen in MRGO-20.

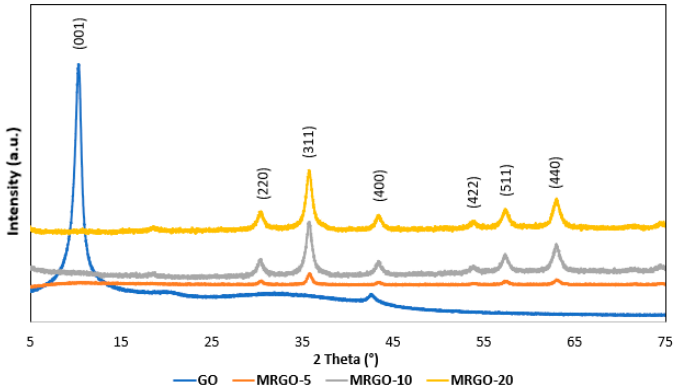

Figure 3. XRD analysis of GO, MRGO-5, MRGO-10 and MRGO-20.

3.2. FESEM Analysis

Figure 4a shows the FESEM images of GO and Figure 4b–d show FESEM images of MRGO-5, MRGO-10 and MRGO-20. As observed from Figure 4a, GO sheets were associated with a rough and irregular wrinkled structure. This might be due to the oxidation of graphite where different oxygen functional groups were being introduced on the surface using the improved Hammer method. Figure 4b–d illustrate that all the Fe_3O_4 deposited on RGO sheets was spherical in shape and well dispersed across the sheets. By introducing Fe_3O_4 nanoparticles on the RGO sheets, the restacking of GO sheets was prevented [23] and the layering of RGO sheets can be well observed in Figure 4b–d. While Fe_3O_4 tends to aggregate, and the tendency would strengthen with increasing loading ratio [24], the deposition on RGO sheets significantly reduced the conglomeration of Fe_3O_4 nanoparticles in all MRGOs samples.

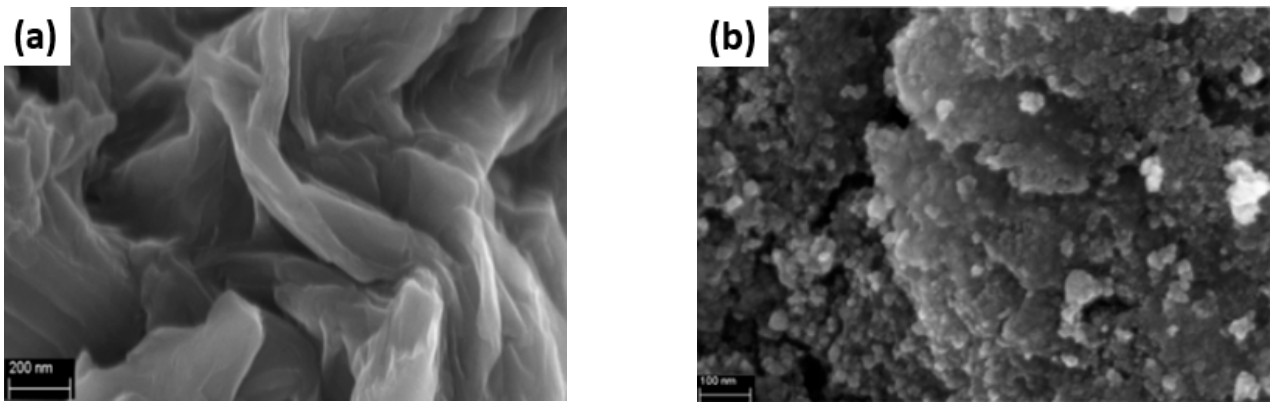

Figure 4. *Cont.*

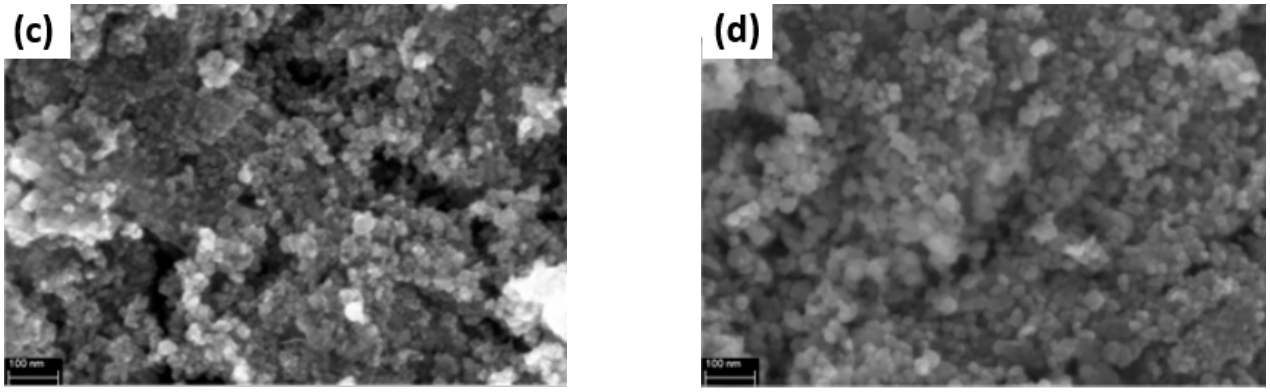

Figure 4. FESEM images of (**a**) GO (**b**) MRGO-5, (**c**) MRGO-10 and (**d**) MRGO-20.

Moreover, as recorded in Table 3, it was observed that as the loading ratio of Fe_3O_4 increases, the weight percentage of Fe increases proportionately as well. The atomic ratio of Fe to C for MRGO-5, MRGO-10 and MRGO-20 was 0.37, 0.71 and 1.27, respectively, increasing in an approximately two-fold manner. As the Fe content is more than C in MRGO-20, and as observed in Figure 4c, the synthesized MRGO was similar to magnetite in appearance which agreed with the XRD results.

Table 3. EDX analysis of GO and MRGOs.

	Element	Weight (%)	Atomic (%)	Atomic Ratio (Fe/c)
GO	C	50.34	57.45	
	O	49.66	42.55	
MRGO-5	C	23.27	38.77	
	O	37.47	46.90	0.37
	Fe	39.26	14.33	
MRGO-10	C	14.12	26.29	
	O	39.42	55.07	0.71
	Fe	46.47	18.64	
MRGO-20	C	9.74	20.85	
	O	32.75	52.65	1.27
	Fe	57.51	26.50	

3.3. Raman Analysis

Figure 5 shows the Raman analysis of GO, MRGO-5, MRGO-10 and MRGO-20. D-band signal and G-band signal of GO was observed at 1369 cm^{-1} and 1585 cm^{-1}, respectively. On the other hand, Raman spectra of MRGO-5, MRGO-10 and MRGO-20 also exhibit a prominent D-band signal around 1353 cm^{-1} and G band signal around 1586 cm^{-1}. D-band signals are related to the sp^3 defects in GO sheets, while G-band signals are related to sp^2 in lane vibration of C-C bond in the RGO sheets [25]. As observed in Figure 5 and recorded in Table 4, the I_D/I_G ratio increased from 0.9625 (GO) to 1.0193 (MRGO-20) after the in situ chemical synthesis. The result indicated the presence of sp^3 reduces within the sp^2 carbon network upon the reduction of GO [26], thereby confirming the formation of RGO sheets in MRGO nanocomposites. It was suggested that the D-band is in fact slightly higher than the G band signal for all MRGOs. Deposition of magnetite through reduction of GO has altered the structure of GO, resulting in higher number of sp^3 defects in the RGO sheets [27]. Furthermore, a magnetite signature was observed around 200–450 cm^{-1} for MRGO-20 [28], specifically at 217 cm^{-1}, 286 cm^{-1} and 393 cm^{-1}, at which the signal at 393 cm^{-1} was due to [OH] groups linked to Fe^{3+} on the magnetite surface [29].

The result strongly suggested the successful deposition of magnetite through redox reaction on the RGO sheets.

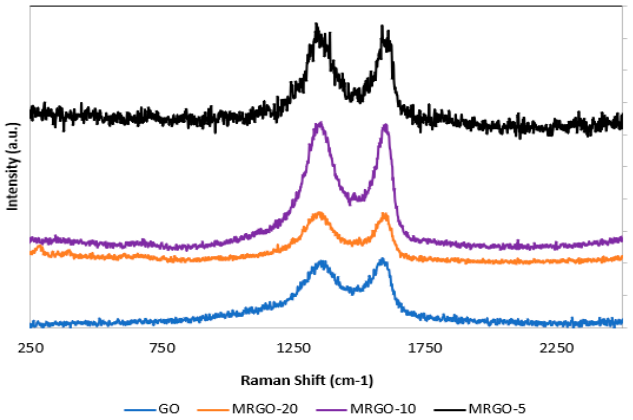

Figure 5. Raman analysis of GO, MRGO-5, MRGO-10 and MRGO-20.

Table 4. I_D/I_G ratio of GO, MRGO-5, MRGO-10 and MRGO-20.

I_D/I_G	GO	MRGO-5	MRGO-10	MRGO-20
	0.9625	1.0077	1.0181	1.0193

3.4. FTIR Analysis

Figure 6 shows the FTIR spectra for GO, MRGO-5, MRGO-10 and MRGO-20. The FTIR spectrum of GO had five characteristic peaks, namely, OH out-of-plane bending at 560 cm^{-1}, CO-O-CO at 1074 cm^{-1}, epoxy C-O at 1218 cm^{-1}, aromatic C=C stretching at 1577 cm^{-1} and hydroxyl (-OH) at 3400 cm^{-1}. The presences of oxygenated functional groups at GO indicated that the graphite underwent oxidation. For MRGO composites, absorption spectrum observed at 3400 cm^{-1} was attributed to the O-H stretching vibration of C-OH group in RGO, while the spectrum at 1577 cm^{-1} was related to the C-OH bending in the RGO sheets [30]. Moreover, a peak was observed at 1220 cm^{-1} suggesting the C-O stretching vibration of epoxy groups or rings in the RGO sheets, and the peak at 618 cm^{-1} was the in-plane deformation vibration of aromatic aldehyde [31]. Notice that the 618 cm^{-1} peak became more significant as the loading ratio of Fe_3O_4 increases, suggesting the deposition of magnetite disrupted the structure of the RGO plane. Lastly, the adsorption peak at 560 cm^{-1} was depicted as the Fe-O vibrations in Fe_3O_4 [32], which increases in absorption intensity as the loading ratio of magnetite increases. This confirmed the interaction between magnetite and RGO sheets. Table 5 shows the comparison of functional groups between GO and MRGOs.

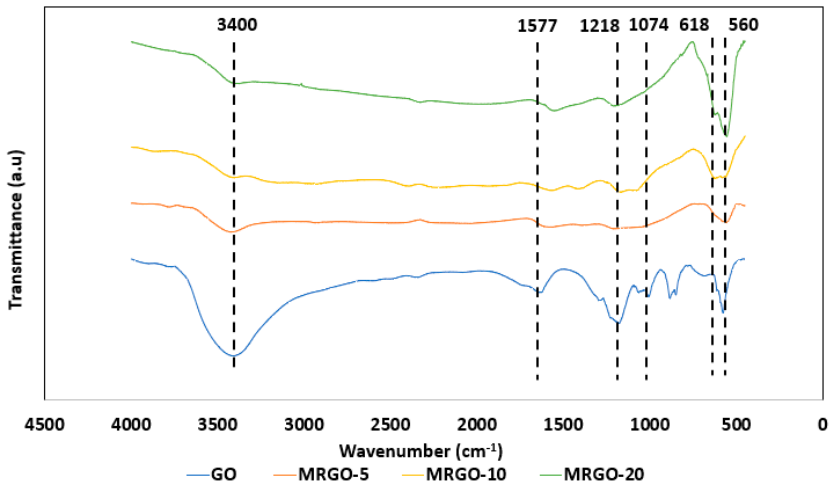

Figure 6. FTIR analysis of GO, MRGO-5, MRG-10 and MRGO-20.

Table 5. FTIR analysis of GO and MrGOs.

Peak Value (cm^{-1})	Functional Groups	GO	MrGO
3400	Hydroxyl-OH	Yes	Yes
1577	Aromatic C=C stretching	Yes	N/A
1218	Epoxy C-O	Yes	Yes
1074	Anhydride group CO-O-CO	Yes	N/A
618	Fe-O	N/A	Yes
560	Fe-O/OH out-of-plane bending	OH out-of-plane bend	Fe-O

3.5. XPS Analysis

Figure 7a shows the wide scan XPS survey of MRGOs where C1s and O1s peaks at binding energies of 285 eV and 530 eV, respectively, were exhibited. As for the peak characteristic of Fe_3O_4, $Fe2p_{3/2}$ and $Fe2p_{1/2}$ peaks were observed at 711 eV and 725 eV, respectively [33]. In Figure 7c,d, deconvolution peaks of C1s show C-C (aromatic) bonds, C-O bonds, C=O bonds and π-π* satellite bonds signal at 285 eV, 287 eV, 289 eV and 291 eV, respectively [34,35]. A signal of π-π* satellite bonds at 291 eV indicates the successful reduction of GO sheets to RGO sheets, as RGO has more sp^2 hybridized zone due to the restoration from the reduction process [35]. The intensity of C1s peak decreases as the loading ratio of Fe_3O_4 increases and is deposited on the RGO sheets. Meanwhile, in Figure 7e,f, deconvolution peaks of O1s indicated Fe-O bonds, C=O bonds and C-O bonds at 530 eV, 531 eV and 533 eV, respectively. The intensity of Fe-O peak at 530 eV was observed to increase significantly for MRGO-20 as more Fe_3O_4 was deposited. Additionally, in both C1s and O1s deconvoluted peaks, C-O peaks were observed to decrease significantly in MRGO-20, which implied an increase in conductivity within the RGO sheets as more sp^2 bonds were restored, thereby enhancing its charge conductivity [36].

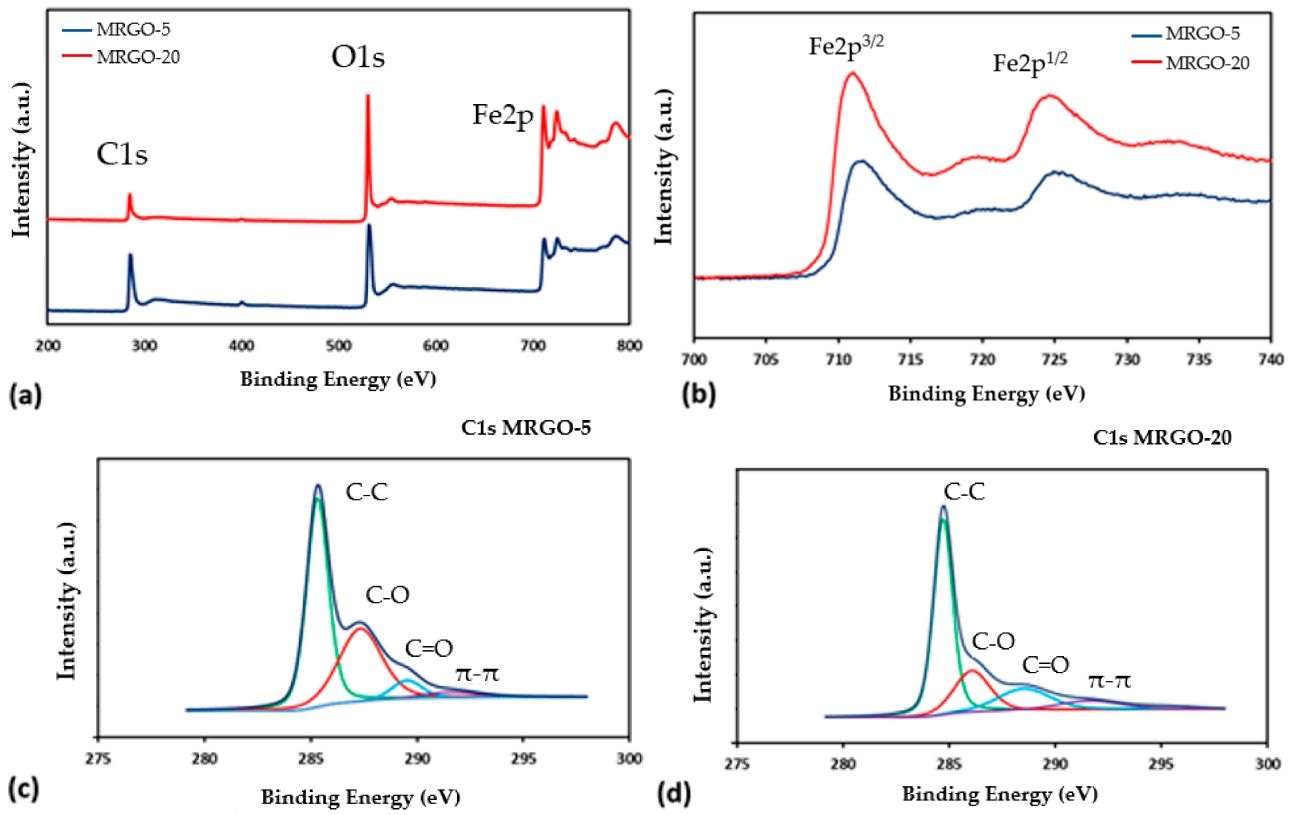

Figure 7. *Cont.*

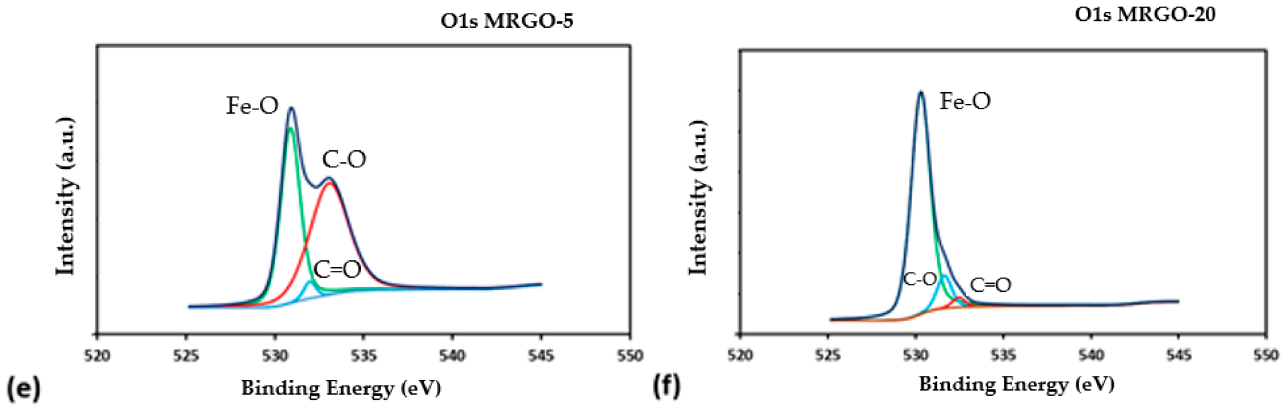

Figure 7. XPS analysis of (**a**) wide scan of MRGO-5 and MRGO-20, (**b**) Fe2p scan of MRGO-5 and MRGO-20, (**c**) C1s scan of MRGO-5, (**d**) C1s scan of MRGO-20, (**e**) O1s scan of MRGO-5 and (**f**) O1s scan of MRGO-20.

3.6. VSM Analysis

Figure 8 shows the VSM magnetization characteristic of MRGO-5 and MRGO-20. MRGO-5 and MRGO-20 exhibit magnetic saturation of 40.7 emu/g and 63.5 emu/g, respectively, inferring the susceptibility to magnetic field is proportionate to the concentration of Fe_3O_4 deposited on the RGO sheets. Further confirming the successful deposition of magnetite on GO sheets through redox reaction at varying ratios. Moreover, the very low coercivity value of the samples indicates that the MRGOs show soft magnetic material features, exhibiting superparamagnetic response and well isolated single domain particle properties [37]. Both have a significant degree of magnetization to allow them to be separated from the emulsion by a magnet after the demulsification process.

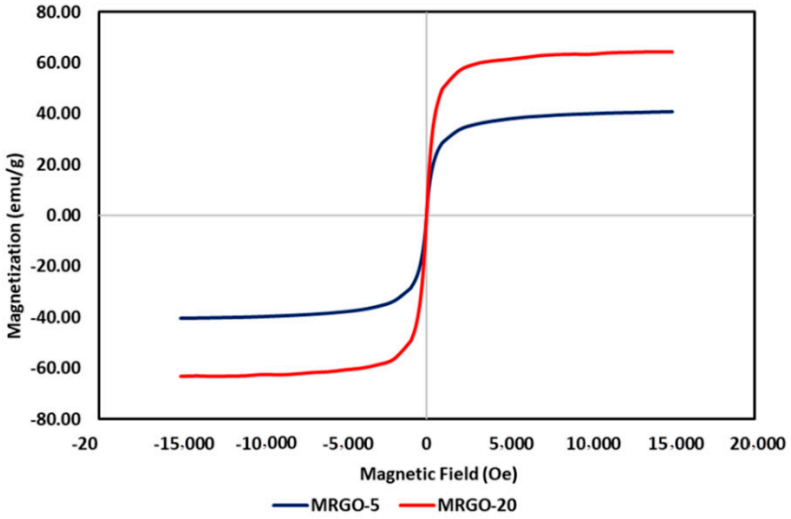

Figure 8. VSM analysis of MRGOs.

3.7. Demulsification Mechanism

Effective demulsification was proposed to be the disruption and breaking up of the interfacial film of Tween 60 between the oil and water interface. The Tween 60 structure has more hydroxyl functional groups, which have adsorptive affinity on Fe_3O_4 nanoparticles [7]. Hence, the demulsification efficiency of MRGOs was seen to increase with the loading ratio of magnetite on RGO sheet when there is no solar irradiance, indicating that Fe_3O_4 nanoparticles played an important role in demulsifying the prepared emulsion.

In Figure 9a, the demulsification efficiency of pure magnetite nanoparticles was about the same across the varying solar intensities, at 42–44% efficiency with a slight increment in

line with the intensity. Pure Fe_3O_4 nanoparticles do not react with visible light wavelength range, hence it is postulated that the slight increment may be due to the following two reasons. (a) Photothermic properties of Fe_3O_4 due to visible light—near infrared spectrum range, which involves micro-heating at the Fe_3O_4 active sites [38]; (b) Fenton-like mechanism due to visible light—ultraviolet spectrum range, which involves the production of oxygen peroxide radicals, O_2 and hydroxyl radicals, OH, from the photocatalytic effect of MRGOs under the influence of solar irradiance [39,40], of which both radicals have high oxidative potential on organic compounds and enhance the demulsification efficiency.

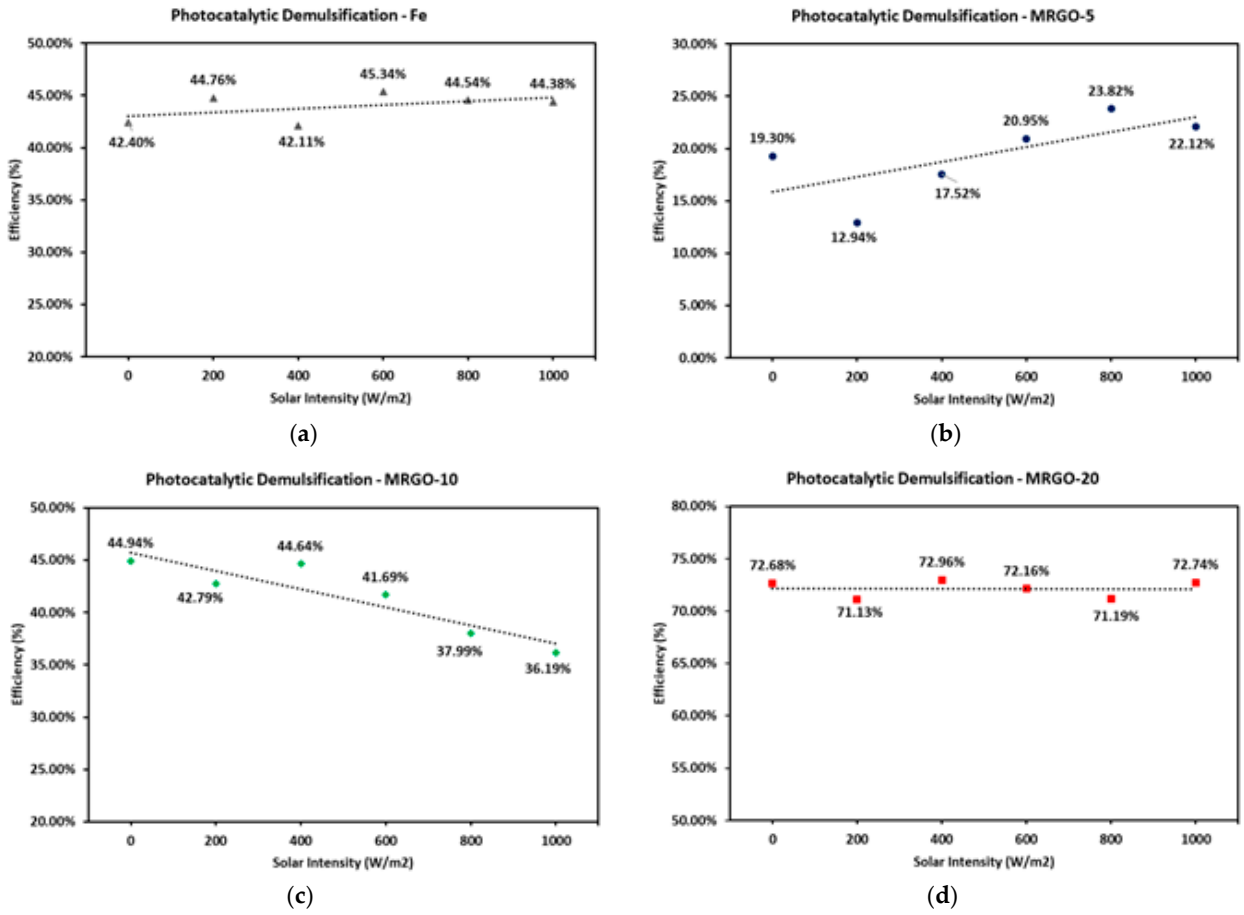

Figure 9. Photocatalytic demulsification using Fe and MRGOs under varying solar intensities.

In Figure 9b, the demulsification efficiency shows an increasing trend with the solar intensity. While the adsorptive capability of MRGO-5 was weak due to a low Fe_3O_4 loading amount, the MRGO nanocomposites show a photocatalytic effect in the demulsification process. The synergy of Fe_3O_4 with RGO sheets augmented the absorption wavelength range of the overall material and facilitated the photocatalytic properties of MRGOs [26]. At the optimum loading ratio of Fe_3O_4, magnetite reacted with the adsorbed hydroxyl group to produce hydroxyl radicals which would further disrupt the oil–water interfacial film of Tween 60 through oxidative reaction [26].

Meanwhile, in Figure 9c, it was expected that the increment in Fe_3O_4 loading amount would improve the demulsification efficiency by increasing the radicals' production [41], but there was an optimum loading amount of Fe_3O_4 for the effective photocatalytic effect to occur [6]. While the adsorption capability of MRGO-10 has shown significant improvement, excess content of Fe_3O_4 introduced new charge recombination at Fe_3O_4, thus reducing the availability of charges within MRGOs [24,42]. That effectively disrupted the affinity of Fe_3O_4 toward hydroxyl group of Tween 60, decreasing the demulsification efficiency.

Figure 9d shows the demulsification efficiency of MRGO-20, at which it was not reactive toward solar irradiance; as magnetite excessively covered most of the RGO sheets, the MRGO nanocomposites behaved similarly to pure magnetite nanoparticles. However, due to the synergy with RGO which prevented the aggregation of Fe_3O_4 nanoparticles, it is suggested that there are more active sites of Fe_3O_4 available for adsorption as compared to pure Fe_3O_4 nanoparticles only. Hence, an enhanced demulsification capability independent of the presence of solar irradiance was observed.

4. Conclusions

Magnetite-reduced graphene oxide nanocomposites were successfully synthesized as verified in the characterization of MRGOs. In the demulsification test, the demulsification efficiency of MRGOs was observed to increase proportionately with the loading amount of Fe_3O_4 on RGO sheets. A positive photocatalytic effect under solar irradiance was observed only with a low loading amount of Fe_3O_4 on RGO sheets, such as in MRGO-5. Hence, it was concluded that while the demulsification efficiency was dependent on the loading amount of Fe_3O_4 on RGO sheets, only a low and optimal loading amount of Fe_3O_4 would show a positive photocatalytic effect.

Author Contributions: Conceptualization, C.S.K. and Z.Y.L.; methodology, Z.Y.L.; validation, C.W.L. and K.Y.Y.; investigation, Z.Y.L. and K.S.T.; resources, W.K.T.; data curation, K.Y.Y.; writing—original draft preparation, Z.Y.L.; writing—review and editing, C.S.K. and K.S.T.; visualization, C.W.L.; supervision, C.S.K. and W.K.T.; funding acquisition, C.S.K. All authors have read and agreed to the published version of the manuscript.

Funding: This research was funded by YUTP fundamental research grant. (015LC0-282) and FRGS (FRGS/1/2019/STG07/UTP/02/6).

Conflicts of Interest: The authors declare no conflict of interest.

References

1. Roodbari, N.H.; Badiei, A.; Soleimani, E.; Khaniani, Y. Tweens demulsification effects on heavy crude oil/water emulsion. *Arab. J. Chem.* **2016**, *9*, S806–S811. [CrossRef]
2. Zolfaghari, R.; Fakhru'l-Razi, A.; Abdullah, L.C.; Elnashaie, S.S.E.H.; Pendashteh, A. Demulsification techniques of water-in-oil and oil-in-water emulsions in petroleum industry. *Sep. Purif. Technol.* **2016**. [CrossRef]
3. Ahmed, S.N.; Haider, W. Heterogeneous photocatalysis and its potential applications in water and wastewater treatment: A review. *Nanotechnology* **2018**, *29*. [CrossRef]
4. Bagheri, S.; Julkapli, N.M. Magnetite hybrid photocatalysis: Advance environmental remediation. *Rev. Inorg. Chem.* **2016**, *36*, 135–151. [CrossRef]
5. Liu, J.; Li, X.; Jia, W.; Li, Z.; Zhao, Y.; Ren, S. Demulsification of Crude Oil-in-Water Emulsions Driven by Graphene Oxide Nanosheets. *Energy Fuels* **2015**, *29*, 4644–4653. [CrossRef]
6. Reza, K.M.; Kurny, A.; Gulshan, F. Photocatalytic Degradation of Methylene Blue by Magnetite+H_2O_2+UV Process. *Int. J. Environ. Sci. Dev.* **2016**, *7*, 325–329. [CrossRef]
7. MArefi; Saberi, D.; Karimi, M.; Heydari, A. Superparamagnetic $Fe(OH)_3$@Fe_3O_4 nanoparticles: An efficient and recoverable catalyst for tandem oxidative amidation of alcohols with amine hydrochloride salts. *ACS Comb. Sci.* **2015**, *17*, 341–347. [CrossRef]
8. Wai, M.M.; Khe, C.S.; Yau, X.H.; Liu, W.W.; Sokkalingam, R.; Jumbri, K.; Lwin, N. Optimization and characterization of magnetite-reduced graphene oxide nanocomposites for demulsification of crude oil in water emulsion. *RSC Adv.* **2019**, *9*, 24003–24014. [CrossRef]
9. Yau, X.H. Synthesis of Magnetite-Reduced Graphene Oxide Nanocomposite as a Recyclable Demulsifier for Crude Oil-In-Water Emulsion. Master's Thesis, University Teknologi Petronus, Perak, Malaysia, 2019.
10. Yau, X.H.; Khe, C.S.; Saheed, M.S.M.; Lai, C.W.; You, K.Y.; Tan, W.K. Magnetically recoverable magnetite-reduced graphene oxide as a demulsifier for surfactant stabilized crude oil-in-water emulsion. *PLoS ONE* **2020**, *15*. [CrossRef] [PubMed]
11. Orimolade, B.O.; Adekola, F.A.; Adebayo, G.B. Adsorptive removal of bisphenol A using synthesized magnetite nanoparticles. *Appl. Water Sci.* **2018**, *8*, 1–8. [CrossRef]
12. Feng, X.; Lou, X. The effect of surfactants-bound magnetite (Fe_3O_4) on the photocatalytic properties of the heterogeneous magnetic zinc oxides nanoparticles. *Sep. Purif. Technol.* **2015**, *147*, 266–275. [CrossRef]
13. Huong, P.T.L.; Huyen, N.T.; Giang, C.D.; Tu, N.; Phan, V.N.; Van Quy, N.; Huy, T.Q.; Hue, D.T.M.; Chinh, H.D.; Le, A.-T. Facile synthesis and excellent adsorption property of GO-Fe_3O_4 magnetic nanohybrids for removal of organic dyes. *J. Nanosci. Nanotechnol.* **2016**, *16*, 9544–9556. [CrossRef]

14. Li, J.; Östling, M. Prevention of graphene restacking for performance boost of supercapacitors-a review. *Crystals* **2013**, *3*, 163–190. [CrossRef]
15. Guo, J.; Jiang, B.; Zhang, X.; Zhou, X.; Hou, W. Fe2.25W0.75O4/reduced graphene oxide nanocomposites for novel bifunctional photocatalyst: One-pot synthesis, magnetically recyclable and enhanced photocatalytic property. *J. Solid State Chem.* **2013**, *205*, 171–176. [CrossRef]
16. Boruah, P.K.; Sharma, B.; Karbhal, I.; Shelke, M.V.; Das, M.R. Ammonia-modified graphene sheets decorated with magnetic Fe_3O_4 nanoparticles for the photocatalytic and photo-Fenton degradation of phenolic compounds under sunlight irradiation. *J. Hazard. Mater.* **2017**, *325*, 90–100. [CrossRef] [PubMed]
17. Sponza, D.T.; Alicanoglu, P. Reuse and recovery of raw hospital wastewater containing ofloxacin after photocatalytic treatment with nano graphene oxide magnetite. *Water Sci. Technol.* **2018**, *77*, 304–322. [CrossRef]
18. Ma, S.; Wang, Y.; Wang, X.; Li, Q.; Tong, S.; Han, X. Bifunctional Demulsifier of ODTS Modified Magnetite/Reduced Graphene Oxide Nanocomposites for Oil–water Separation. *ChemistrySelect* **2016**, *1*, 4742–4746. [CrossRef]
19. Wang, B.; Gu, D.; Ji, L.; Wu, H. Photocatalysis: A novel approach to efficient demulsification. *Catal. Commun.* **2016**, *75*, 83–86. [CrossRef]
20. Teo, P.S.; Lim, H.N.; Huang, N.M.; Chia, C.H.; Harrison, I. Room temperature in situ chemical synthesis of Fe_3O_4/graphene. *Ceram. Int.* **2012**, *38*, 6411–6416. [CrossRef]
21. Chia, C.H. Fabrication and characterization of graphene hydrogel via hydrothermal approach as a scaffold for preliminary study of cell growth. *Int. J. Nanomed.* **2011**, *6*, 1817–1823.
22. Di Iorio, E.; Colombo, C.; Cheng, Z.; Capitani, G.; Mele, D.; Ventruti, G.; Angelico, R. Characterization of magnetite nanoparticles synthetized from Fe(II)/nitrate solutions for arsenic removal from water. *J. Environ. Chem. Eng.* **2019**, *7*, 102986. [CrossRef]
23. Xu, C.; Wang, X.; Zhu, J. Graphene-Metal particle nanocomposites. *J. Phys. Chem. C* **2008**, *112*, 19841–19845. [CrossRef]
24. Peik-See, T.; Pandikumar, A.; Ngee, L.H.; Ming, H.N.; Hua, C.C. Magnetically separable reduced graphene oxide/iron oxide nanocomposite materials for environmental remediation. *Catal. Sci. Technol.* **2014**, *4*, 4396–4405. [CrossRef]
25. Hidayah, N.M.S.; Liu, W.-W.; Lai, C.-W.; Noriman, N.Z.; Khe, C.-S.; Hashim, U.; Lee, H.C. Comparison on graphite, graphene oxide and reduced graphene oxide: Synthesis and characterization. *AIP Conf. Proc.* **2017**, *1892*. [CrossRef]
26. Moztahida, M.; Jang, J.; Nawaz, M.; Lim, S.R.; Lee, D.S. Effect of rGO loading on Fe_3O_4: A visible light assisted catalyst material for carbamazepine degradation. *Sci. Total Environ.* **2019**, *667*, 741–750. [CrossRef] [PubMed]
27. Wu, J.B.; Lin, M.L.; Cong, X.; Liu, H.N.; Tan, P.H. Raman spectroscopy of graphene-based materials and its applications in related devices. *Chem. Soc. Rev.* **2018**, *47*, 1822–1873. [CrossRef]
28. Shebanova, O.N.; Lazor, P. Raman spectroscopic study of magnetite ($FeFe_2O_4$): A new assignment for the vibrational spectrum. *J. Solid State Chem.* **2003**, *174*, 424–430. [CrossRef]
29. Slavov, L.; Abrashev, M.; Merodiiska, T.; Gelev, C.; Vandenberghe, R.; Markova-Deneva, I.; Nedkov, I. Raman spectroscopy investigation of magnetite nanoparticles in ferrofluids. *J. Magn. Magn. Mater.* **2010**, *322*, 1904–1911. [CrossRef]
30. Andrijanto, E.; Shoelarta, S.; Subiyanto, G.; Rifki, S. Facile synthesis of graphene from graphite using ascorbic acid as reducing agent. *AIP Conf. Proc.* **2016**, *1725*. [CrossRef]
31. Zhou, Z.; Su, M.; Shih, K. Highly efficient and recyclable graphene oxide-magnetite composites for isatin mineralization. *J. Alloy. Compd.* **2017**, *725*, 302–309. [CrossRef]
32. Akbarzadeh, A.; Samiei, M.; Joo, S.W.; Anzaby, M.; Hanifehpour, Y. RETRACTED ARTICLE: Synthesis, characterization and in vitro studies of doxorubicin-loaded magnetic nanoparticles grafted to smart copolymers on A549 lung cancer cell line. *J. Nanobiotechnol.* **2012**, 1–13. [CrossRef]
33. Yamashita, T.; Hayes, P. Analysis of XPS spectra of Fe^{2+} and Fe^{3+} ions in oxide materials. *Appl. Surf. Sci.* **2008**, *254*, 2441–2449. [CrossRef]
34. Muzyka, R.; Drewniak, S.; Pustelny, T.; Chrubasik, M.; Gryglewicz, G. Characterization of graphite oxide and reduced graphene oxide obtained from different graphite precursors and oxidized by different methods using Raman spectroscopy. *Materials* **2018**, *11*, 1050. [CrossRef] [PubMed]
35. Al-Gaashani, R.; Najjar, A.; Zakaria, Y.; Mansour, S.; Atieh, M.A. XPS and structural studies of high quality graphene oxide and reduced graphene oxide prepared by different chemical oxidation methods. *Ceram. Int.* **2019**, *45*, 14439–14448. [CrossRef]
36. Xu, C.; Shi, X.; Ji, A.; Shi, L.; Zhou, C.; Cui, Y. Fabrication and characteristics of reduced graphene oxide produced with different green reductants. *PLoS ONE* **2015**, *10*. [CrossRef]
37. Lu, A.H.; Salabas, E.L.; Schüth, F. Magnetic nanoparticles: Synthesis, protection, functionalization, and application. *Angew. Chem. Int. Ed.* **2007**, *46*, 1222–1244. [CrossRef]
38. Pang, F.; Zhang, R.; Lan, D.; Ge, J. Synthesis of Magnetite-Semiconductor-Metal Trimer Nanoparticles through Functional Modular Assembly: A Magnetically Separable Photocatalyst with Photothermic Enhancement for Water Reduction. *ACS Appl. Mater. Interfaces* **2018**, *10*, 4929–4936. [CrossRef] [PubMed]
39. Wang, X.; Tian, H.; Yang, Y.; Wang, H.; Wang, S.; Zheng, W.; Liu, Y. Reduced graphene oxide/CdS for efficiently photocatalystic degradation of methylene blue. *J. Alloy. Compd.* **2012**, *524*, 5–12. [CrossRef]
40. Jiang, X.; Li, L.; Cui, Y.; Cui, F. New branch on old tree: Green-synthesized RGO/Fe_3O_4 composite as a photo-Fenton catalyst for rapid decomposition of methylene blue. *Ceram. Int.* **2017**, *43*, 14361–14368. [CrossRef]

41. Liu, W.; Qian, J.; Wang, K.; Xu, H.; Jiang, D.; Liu, Q.; Yang, X.; Li, H. Magnetically Separable Fe_3O_4 Nanoparticles-Decorated Reduced Graphene Oxide Nanocomposite for Catalytic Wet Hydrogen Peroxide Oxidation. *J. Inorg. Organomet. Polym. Mater.* **2013**, *23*, 907–916. [CrossRef]
42. Mahapatra, P.; Giri, S.K.; Das, N. Adsorptive and photocatalytic remediation of aqueous organic dyes and chromium(VI) by manganese(II) substituted magnetite nanoparticles. *Desalin. Water Treat.* **2019**, *141*, 208–219. [CrossRef]